A measurement of the mean lifetimes
of charged and neutral *B*-hadrons

DELPHI Collaboration

P. Abreu[t], W. Adam[g], T. Adye[ak], E. Agasi[ad], I. Ajinenko[aq], R. Aleksan[am], G.D. Alekseev[n], A. Algeri[m], P. Allen[aw], S. Almehed[w], S.J. Alvsvaag[d], U. Amaldi[g], A. Andreazza[aa], P. Antilogus[x], W-D. Apel[o], R.J. Apsimon[ak], Y. Arnoud[am], B. Åsman[as], J-E. Augustin[r], A. Augustinus[ad], P. Baillon[g], P. Bambade[r], F. Barao[t], R. Barate[ℓ], G. Barbiellini[au], D.Y. Bardin[n], G.J. Barker[ah], A. Baroncelli[ao], O. Barring[g], J.A. Barrio[y], W. Bartl[ay], M.J. Bates[ak], M. Battaglia[m], M. Baubillier[v], K-H. Becks[ba], C.J. Beeston[ah], M. Begalli[aj], P. Beilliere[f], Yu. Belokopytov[aq], P. Beltran[i], D. Benedic[h], A.C. Benvenuti[e], M. Berggren[r], D. Bertrand[b], F. Bianchi[at], M.S. Bilenky[n], P. Billoir[v], J. Bjarne[w], D. Bloch[h], S. Blyth[ah], V. Bocci[aℓ], P.N. Bogolubov[n], T. Bolognese[am], M. Bonesini[aa], W. Bonivento[aa], P.S.L. Booth[u], G. Borisov[aq], H. Borner[g], C. Bosio[ao], B. Bostjancic[ar], S. Bosworth[ah], O. Botner[av], B. Bouquet[r], C. Bourdarios[r], T.J.V. Bowcock[u], M. Bozzo[k], S. Braibant[b], P. Branchini[ao], K.D. Brand[ai], R.A. Brenner[g], H. Briand[v], C. Bricman[b], R.C.A. Brown[g], N. Brummer[ad], J-M. Brunet[f], L. Bugge[af], T. Buran[af], H. Burmeister[g], J.A.M.A. Buytaert[g], M. Caccia[g], M. Calvi[aa], A.J. Camacho Rozas[ap], R. Campion[u], T. Camporesi[g], V. Canale[aℓ], F. Cao[b], F. Carena[g], L. Carroll[u], C. Caso[k], M.V. Castillo Gimenez[aw], A. Cattai[g], F.R. Cavallo[e], L. Cerrito[aℓ], V. Chabaud[g], A. Chan[a], Ph. Charpentier[g], L. Chaussard[r], J. Chauveau[v], P. Checchia[ai], G.A. Chelkov[n], L. Chevalier[am], P. Chliapnikov[aq], V. Chorowicz[v], J.T.M. Chrin[aw], P. Collins[ah], J.L. Contreras[y], R. Contri[k], E. Cortina[aw], G. Cosme[r], F. Couchot[r], H.B. Crawley[a], D. Crennell[ak], G. Crosetti[k], M. Crozon[f], J. Cuevas Maestro[ag], S. Czellar[m], E. Dahl-Jensen[ab], B. Dalmagne[r], M. Dam[af], G. Damgaard[ab], E. Daubie[b], A. Daum[o], P.D. Dauncey[ah], M. Davenport[g], P. David[v], J. Davies[u], W. Da Silva[v], C. Defoix[f], P. Delpierre[f], N. Demaria[at], A. De Angelis[au], H. De Boeck[b], W. De Boer[o], C. De Clercq[b], M.D.M. De Fez Laso[aw], N. De Groot[ad], C. De La Vaissiere[v], B. De Lotto[au], A. De Min[aa], H. Dijkstra[g], L. Di Ciaccio[aℓ], J. Dolbeau[f], M. Donszelmann[g], K. Doroba[az], M. Dracos[g], J. Drees[ba], M. Dris[ae], Y. Dufour[g], F. Dupont[ℓ], D. Edsall[a], L-O. Eek[av], P.A.-M. Eerola[g], R. Ehret[o], T. Ekelof[av], G. Ekspong[as], A. Elliot Peisert[ai], J-P. Engel[h], N. Ershaidat[v], V. Falaleev[aq], D. Fassouliotis[ae], M. Feindt[g], M. Fernandez Alonso[ap], A. Ferrer[aw], T.A. Filippas[ae], A. Firestone[a], H. Foeth[g], E. Fokitis[ae], F. Fontanelli[k], K.A.J. Forbes[u], J-L. Fousset[z], S. Francon[x], B. Franek[ak], P. Frenkiel[f], D.C. Fries[o], A.G. Frodesen[d], R. Fruhwirth[ay], F. Fulda-Quenzer[r], K. Furnival[u], H. Furstenau[o], J. Fuster[g], D. Gamba[at], C. Garcia[aw], J. Garcia[ap], C. Gaspar[g], U. Gasparini[ai], Ph. Gavillet[g], E.N. Gazis[ae], J-P. Gerber[h], P. Giacomelli[g], R. Gokieli[az], B. Golob[ar], V.M. Golovatyuk[n], J.J. Gomez Y Cadenas[g], G. Gopal[ak], L. Gorn[a], M. Gorski[az], V. Gracco[k], A. Grant[g], F. Grard[b], E. Graziani[ao], G. Grosdidier[r], E. Gross[g], P. Grosse-Wiesmann[g], B. Grossetete[v], J. Guy[ak], U. Haedinger[o], F. Hahn[ba], M. Hahn[o], S. Haider[ad], A. Hakansson[w], A. Hallgren[av], K. Hamacher[ba], G. Hamel De Monchenault[am], W. Hao[ad], F.J. Harris[ah], V. Hedberg[w], T. Henkes[g], J.J. Hernandez[aw], P. Herquet[b], H. Herr[g], T.L. Hessing[u], I. Hietanen[m], C.O. Higgins[u], E. Higon[aw], H.J. Hilke[g], S.D. Hodgson[ah], T. Hofmokl[az], S-O. Holmgren[as], D. Holthuizen[ad], P.F. Honore[f], J.E. Hooper[ab], M. Houlden[u], J. Hrubec[ay],

K. Huet [b], P.O. Hulth [as], K. Hultqvist [as], P. Ioannou [c], P-S. Iversen [d], J.N. Jackson [u], P. Jalocha [p],
G. Jarlskog [w], P. Jarry [am], B. Jean-Marie [r], E.K. Johansson [as], D. Johnson [u], M. Jonker [g],
L. Jonsson [w], P. Juillot [h], G. Kalkanis [c], G. Kalmus [ak], F. Kapusta [v], M. Karlsson [g], E. Karvelas [i],
S. Katsanevas [c], E.C. Katsoufis [ae], R. Keranen [g], J. Kesteman [b], B.A. Khomenko [n],
N.N. Khovanski [n], B. King [u], N.J. Kjaer [g], H. Klein [g], A. Klovning [d], P. Kluit [ad],
A. Koch-Mehrin [ba], J.H. Koehne [o], B. Koene [ad], P. Kokkinias [i], M. Koratzinos [af], A.V. Korytov [n],
V. Kostioukhine [aq], C. Kourkoumelis [c], O. Kouznetsov [n], P.H. Kramer [ba], C. Kreuter [o],
J. Krolikowski [az], I. Kronkvist [w], U. Kruener-Marquis [ba], W. Krupinski [p], K. Kulka [av],
K. Kurvinen [m], C. Lacasta [aw], C. Lambropoulos [i], J.W. Lamsa [a], L. Lanceri [au], V. Lapin [aq],
J-P. Laugier [am], R. Lauhakangas [m], G. Leder [ay], F. Ledroit [ℓ], R. Leitner [ac], Y. Lemoigne [am],
J. Lemonne [b], G. Lenzen [ba], V. Lepeltier [r], T. Lesiak [p], J.M. Levy [h], E. Lieb [ba], D. Liko [ay],
J. Lindgren [m], R. Lindner [ba], A. Lipniacka [az], I. Lippi [ai], B. Loerstad [w], M. Lokajicek [j],
J.G. Loken [ah], A. Lopez-Fernandez [g], M.A. Lopez Aguera [ap], M. Los [ad], D. Loukas [i],
J.J. Lozano [aw], P. Lutz [f], L. Lyons [ah], G. Maehlum [af], J. Maillard [f], A. Maio [t], A. Maltezos [i],
F. Mandl [ay], J. Marco [ap], M. Margoni [ai], J-C. Marin [g], A. Markou [i], T. Maron [ba], S. Marti [aw],
F. Matorras [ap], C. Matteuzzi [aa], G. Matthiae [aℓ], M. Mazzucato [ai], M. Mc Cubbin [u], R. Mc Kay [a],
R. Mc Nulty [u], G. Meola [k], C. Meroni [aa], W.T. Meyer [a], M. Michelotto [ai], I. Mikulec [ay],
L. Mirabito [x], W.A. Mitaroff [ay], G.V. Mitselmakher [n], U. Mjoernmark [w], T. Moa [as], R. Moeller [ab],
K. Moenig [g], M.R. Monge [k], P. Morettini [k], H. Mueller [o], W.J. Murray [ak], B. Muryn [p],
G. Myatt [ah], F.L. Navarria [e], P. Negri [aa], R. Nicolaidou [c], B.S. Nielsen [ab], B. Nijjhar [u],
V. Nikolaenko [aq], P.E.S. Nilsen [d], P. Niss [as], A. Nomerotski [ai], V. Obraztsov [aq], A.G. Olshevski [n],
R. Orava [m], A. Ostankov [aq], K. Osterberg [m], A. Ouraou [am], M. Paganoni [aa], R. Pain [v], H. Palka [p],
Th.D. Papadopoulou [ae], L. Pape [g], F. Parodi [k], A. Passeri [ao], M. Pegoraro [ai], J. Pennanen [m],
L. Peralta [t], H. Pernegger [ay], M. Pernicka [ay], A. Perrotta [e], C. Petridou [au], A. Petrolini [k],
F. Pierre [am], M. Pimenta [t], O. Pingot [b], S. Plaszczynski [r], O. Podobrin [o], M.E. Pol [q], G. Polok [p],
P. Poropat [au], V. Pozdniakov [n], P. Privitera [o], A. Pullia [aa], D. Radojicic [ah], S. Ragazzi [aa],
H. Rahmani [ae], P.N. Ratoff [s], A.L. Read [af], P. Rebecchi [g], N.G. Redaelli [aa], M. Regler [ay], D. Reid [g],
P.B. Renton [ah], L.K. Resvanis [c], F. Richard [r], M. Richardson [u], J. Ridky [j], G. Rinaudo [at],
I. Roditi [q], A. Romero [at], I. Roncagliolo [k], P. Ronchese [ai], C. Ronnqvist [m], E.I. Rosenberg [a],
S. Rossi [g], E. Rosso [g], P. Roudeau [r], T. Rovelli [e], W. Ruckstuhl [ad], V. Ruhlmann-Kleider [am],
A. Ruiz [ap], K. Rybicki [p], H. Saarikko [m], Y. Sacquin [am], G. Sajot [ℓ], J. Salt [aw], J. Sanchez [y],
M. Sannino [k,an], S. Schael [g], H. Schneider [o], M.A.E. Schyns [ba], G. Sciolla [at], F. Scuri [au],
A.M. Segar [ah], A. Seitz [o], R. Sekulin [ak], M. Sessa [au], R. Seufert [o], R.C. Shellard [aj], I. Siccama [ad],
P. Siegrist [am], S. Simonetti [k], F. Simonetto [ai], A.N. Sisakian [n], G. Skjevling [af], G. Smadja [am,x],
N. Smirnov [aq], O. Smirnova [n], G.R. Smith [ak], R. Sosnowski [az], D. Souza-Santos [aj], T.S. Spassoff [ℓ],
E. Spiriti [ao], S. Squarcia [k], H. Staeck [ba], C. Stanescu [ao], S. Stapnes [af], G. Stavropoulos [i],
F. Stichelbaut [b], A. Stocchi [r], J. Strauss [ay], J. Straver [g], R. Strub [h], B. Stugu [d], M. Szczekowski [g],
M. Szeptycka [az], P. Szymanski [az], T. Tabarelli [aa], O. Tchikilev [aq], G.E. Theodosiou [i], A. Tilquin [z],
J. Timmermans [ad], V.G. Timofeev [n], L.G. Tkatchev [n], T. Todorov [h], D.Z. Toet [ad], O. Toker [m],
B. Tome [t], E. Torassa [at], L. Tortora [ao], D. Treille [g], W. Trischuk [g], G. Tristram [f], C. Troncon [aa],
A. Tsirou [g], E.N. Tsyganov [n], M. Turala [p], M-L. Turluer [am], T. Tuuva [m], I.A. Tyapkin [v],
M. Tyndel [ak], S. Tzamarias [u], S. Ueberschaer [ba], O. Ullaland [g], V. Uvarov [aq], G. Valenti [e],
E. Vallazza [at], J.A. Valls Ferrer [aw], C. Vander Velde [b], G.W. Van Apeldoorn [ad], P. Van Dam [ad],
M. Van Der Heijden [ad], W.K. Van Doninck [b], P. Vaz [g], G. Vegni [aa], L. Ventura [ai], W. Venus [ak],
F. Verbeure [b], M. Verlato [ai], L.S. Vertogradov [n], D. Vilanova [am], P. Vincent [x], L. Vitale [m],
E. Vlasov [aq], A.S. Vodopyanov [n], M. Vollmer [ba], M. Voutilainen [m], V. Vrba [ao], H. Wahlen [ba],
C. Walck [as], F. Waldner [au], A. Wehr [ba], M. Weierstall [ba], P. Weilhammer [g], J. Werner [ba],

A.M. Wetherell [g], J.H. Wickens [b], G.R. Wilkinson [ah], W.S.C. Williams [ah], M. Winter [h],
M. Witek [p], G. Wormser [r], K. Woschnagg [av], N. Yamdagni [as], P. Yepes [g], A. Zaitsev [aq],
A. Zalewska [p], P. Zalewski [r], D. Zavrtanik [ar], E. Zevgolatakos [i], G. Zhang [ba], N.I. Zimin [n],
M. Zito [am], R. Zuberi [ah], R. Zukanovich Funchal [f], G. Zumerle [ai] and J. Zuniga [aw]

[a] *Ames Laboratory and Department of Physics, Iowa State University, Ames IA 50011, USA*
[b] *Physics Department, Universitaire Instelling Antwerpen, Universiteitsplein 1, B-2610 Wilrijk, Belgium*
  and IIHE, ULB-VUB, Pleinlaan 2, B-1050 Brussels, Belgium
  and Faculté des Sciences, Université de l'Etat Mons, Av. Maistriau 19, B-7000 Mons, Belgium
[c] *Physics Laboratory, University of Athens, Solonos Street 104, GR-10680 Athens, Greece*
[d] *Department of Physics, University of Bergen, Allégaten 55, N-5007 Bergen, Norway*
[e] *Dipartimento di Fisica, Università di Bologna and INFN, Via Irnerio 46, I-40126 Bologna, Italy*
[f] *Collège de France, Laboratoire de Physique Corpusculaire, IN2P3–CNRS, F-75231 Paris Cedex 05, France*
[g] *CERN, CH-1211 Geneva 23, Switzerland*
[h] *Centre de Recherche Nucléaire, IN2P3–CNRS/ULP, B.P. 20, F-67037 Strasbourg Cedex, France*
[i] *Institute of Nuclear Physics, NCSR Demokritos, P.O. Box 60228, GR-15310 Athens, Greece*
[j] *FZU, Institute of Physics of the C.A.S. High Energy Physics Division,*
  Na Slovance 2, CS-180 40, Praha 8, Czech Republic
[k] *Dipartimento di Fisica, Università di Genova and INFN, Via Dodecaneso 33, I-16146 Genova, Italy*
[l] *Institut des Sciences Nucléaires, IN2P3–CNRS, Université de Grenoble 1, F-38026 Grenoble, France*
[m] *Research Institute for High Energy Physics, SEFT, Siltavuorenpenger 20 C, SF-00170 Helsinki, Finland*
[n] *Joint Institute for Nuclear Research, Dubna, Head Post Office, P.O. Box 79, 101 000 Moscow, Russian Federation*
[o] *Institut für Experimentelle Kernphysik, Universität Karlsruhe, Pf. 6980, D-7500 Karlsruhe 1, Germany*
[p] *High Energy Physics Laboratory, Institute of Nuclear Physics, Ul. Kawiory 26 a, PL-30055 Krakow 30, Poland*
[q] *Centro Brasileiro de Pesquisas Fisicas, rua Xavier Sigaud 150, RJ-22290 Rio de Janeiro, Brazil*
[r] *Université de Paris-Sud, Laboratoire de l'Accélérateur Linéaire, IN2P3–CNRS, Bâtiment 200, F-91405 Orsay, France*
[s] *School of Physics and Materials, University of Lancaster, GB - Lancaster LA1 4YB, UK*
[t] *LIP, IST, FCUL, Av. Elias Garcia, 14 - 1o, P-1000 Lisboa Codex, Portugal*
[u] *Department of Physics, University of Liverpool, P.O. Box 147, GB - Liverpool L69 3BX, UK*
[v] *LPNHE, IN2P3–CNRS, Universités Paris VI et VII, Tour 33 (RdC), 4 place Jussieu, F-75252 Paris Cedex 05, France*
[w] *Department of Physics, University of Lund, Sölvegatan 14, S-22363 Lund, Sweden*
[x] *Université Claude Bernard de Lyon, IPNL, IN2P3–CNRS, F-69622 Villeurbanne Cedex, France*
[y] *Universidad Complutense, Avda. Complutense s/n, E-28040 Madrid, Spain*
[z] *Université d'Aix – Marseille II – CPP, IN2P3–CNRS, F-13288 Marseille Cedex 09, France*
[aa] *Dipartimento di Fisica, Università di Milano and INFN, Via Celoria 16, I-20133 Milan, Italy*
[ab] *Niels Bohr Institute, Blegdamsvej 17, DK-2100 Copenhagen Ø, Denmark*
[ac] *NC, Nuclear Centre of MFF, Charles University, Areal MFF, V Holesovickach 2, CS-180 00, Praha 8, Czech Republic*
[ad] *NIKHEF-H, Postbus 41882, NL-1009 DB Amsterdam, The Netherlands*
[ae] *National Technical University, Physics Department, Zografou Campus, GR-15773 Athens, Greece*
[af] *Physics Department, University of Oslo, Blindern, N-1000 Oslo 3, Norway*
[ag] *Departamento Fisica, Universidad Oviedo, C/P.Jimenez Casas, S/N-33006 Oviedo, Spain*
[ah] *Department of Physics, University of Oxford, Keble Road, Oxford OX1 3RH, UK*
[ai] *Dipartimento di Fisica, Università di Padova and INFN, Via Marzolo 8, I-35131 Padua, Italy*
[aj] *Departamento de Fisica, Pontificia Universidade Católica, C.P. 38071, RJ-22453 Rio de Janeiro, Brazil*
[ak] *Rutherford Appleton Laboratory, Chilton, GB - Didcot OX11 OQX, UK*
[al] *Dipartimento di Fisica, Università di Roma II and INFN, Tor Vergata, I-00173 Rome, Italy*
[am] *Centre d'Etude de Saclay, DSM/DAPNIA, F-91191 Gif-sur-Yvette Cedex, France*
[an] *Dipartimento di Fisica, Università di Salerno, I-84100 Salerno, Italy*
[ao] *Istituto Superiore di Sanità, INFN, Viale Regina Elena 299, I-00161 Rome, Italy*
[ap] *CEAFM, CSIC, Universidad Cantabria, Avda. los Castros, S/N-39006 Santander, Spain*
[aq] *Institute for High Energy Physics, Serpukov, P.O. Box 35, Protvino (Moscow Region), Russian Federation*
[ar] *J. Stefan Institute and Department of Physics, University of Ljubljana, Jamova 39, SI-61000 Ljubljana, Slovenia*
[as] *Fysikum, Stockholm University, Box 6730, S-113 85 Stockholm, Sweden*
[at] *Dipartimento di Fisica Sperimentale, Università di Torino and INFN, Via P. Giuria 1, I-10125 Turin, Italy*
[au] *Dipartimento di Fisica, Università di Trieste and INFN, Via A. Valerio 2, I-34127 Trieste, Italy*
  and Istituto di Fisica, Università di Udine, I-33100 Udine, Italy

[av] *Department of Radiation Sciences, University of Uppsala, P.O. Box 535, S-751 21 Uppsala, Sweden*

[aw] *IFIC, Valencia–CSIC, and DFAMN, Universidad de Valencia,*
 Avda. Dr. Moliner 50, E-46100 Burjassot (Valencia), Spain

[ay] *Institut für Hochenergiephysik, Österreichische Akademie der Wissenschaften,*
 Nikolsdorfergasse 18, A-1050 Vienna, Austria

[az] *Institute of Nuclear Studies and University of Warsaw, Ul. Hoza 69, PL-00681 Warsaw, Poland*

[ba] *Fachbereich Physik, Universität Wuppertal, Pf. 100 127, D-5600 Wuppertal 1, Germany*

The decays of B-hadrons have been reconstructed using the charged particles recorded in the DELPHI silicon microstrip detector. The sum of the charges of the secondaries determines the charge of the B-hadron parent. Some 232 114 multihadronic Z^0 decays recorded during the 1991 run of LEP at centre-of-mass energies between 88.2 GeV and 94.2 GeV yield 253 B-hadron candidates with well-measured charge. From these the mean lifetimes of neutral and charged B-hadrons are found to be 1.44 ± 0.21(stat.) ± 0.14(syst.) ps and 1.56 ± 0.19(stat.) ± 0.13(syst.) ps respectively. The ratio of their lifetimes is $1.09^{+0.28}_{-0.23}$(stat.) ± 0.11(syst.). Under some assumptions on the abundance and lifetime of the Λ^0_b and B^0_s states, the B^0 and B^+ lifetimes are inferred.

1. Introduction

The aim of this analysis is to measure the charged and neutral B-hadron lifetimes using the event topology, without explicit identification of the final states. The method is entirely dependent upon finding the production and decay vertices using the charged particle tracks, and therefore relies largely upon the vertex detector of DELPHI to identify which charged particles come from a secondary vertex, and hence to ensure that the B charge [#1] is well estimated.

According to the spectator model [1], the light constituents are expected to play a passive role in weak decays of hadrons composed of a heavy quark and light quarks. This model predicts that the lifetimes of all weak decays with a heavy quark are equal and are determined by the lifetime of the heavy quark. However, the lifetime differences between charmed particles clearly indicate corrections to the spectator model.

A brief description of the detector can be found in section 2. Section 3 details the event selection procedure and section 4 describes the fit technique. The B lifetime results are presented in section 5.

2. The apparatus

The DELPHI detector has been described in detail elsewhere [2]. Only the properties relevant to this analysis are summarized here.

In the barrel region, charged particles are measured by a set of cylindrical tracking detectors whose z axes are common with the beam direction and with the axis of the solenoidal magnet which produces a 1.23 T field. The coordinate system is defined by the azimuthal angle ϕ and the radius R from the axis, and either the polar angle θ to the electron beam direction, or the z distance along that direction.

The Time Projection Chamber (TPC) is the main tracking device. Charged particles tracks are reconstructed in three dimensions for radii between 30 cm and 122 cm with up to 16 space points for polar angles between 39° and 141°, and four or more space points for polar angles between 21° and 39° and between 141° and 159°.

Additional measurements are provided by the inner and outer detectors. The inner detector (ID) is a cylindrical drift chamber covering radii between 12 cm and 28 cm and θ between 29° and 151°. A central jet chamber giving up to 24 $R\phi$ coordinates is surrounded by five layers of proportional chambers providing both $R\phi$ and z coordinates. The outer detector has five layers of drift cells at radii between 198 cm and 206 cm and θ between 42° and 138°.

[#1] The symbol B means charged or neutral B-hadron.

The vertex detector (VD) [3] used in this analysis consisted of two independent half shells of silicon microstrip detectors inserted between the beam pipe an the ID. Each half shell had three concentric and overlapping layers of silicon microstrip detectors located at average radii 6.3 cm, 8.8 cm and 10.9 cm. The overlap between detectors in a layer was about 10%; the split between the two half-shells also had this overlap.

The vertex detector measured three $R\phi$ coordinates for particles with polar angle between 43° and 137°. The intrinsic precision of the microstrip detectors was measured to be 6 μm and the precision of a $R\phi$ measurement on a charged particle was 8 μm. A three-dimensional survey of the sensitive elements (with a precision in $R\phi$ of 20 μm) provided the alignment prior to installation. The final alignment used Z^0 decays into muon pairs or hadronic final states. Particles passing through the overlapping VD layers were used as a cross-check on this alignment. Fibre optic and capacitive devices monitored the stability of the detector during the data-taking and showed the maximum movements of the detector to be less than 10 μm.

To measure charged particle tracks accurately needed a combination of VD, ID, TPC and OD detectors. In particular the vertex detector precision alone was not sufficient to measure accurately the particle momenta, or even the charges. Tracks from one detector were thus associated to the next component, a procedure which in general started from the TPC tracks, and an overall track fit was applied to each particle.

The position and size of the LEP beam was found on a run by run basis, as described in ref. [4]. The mean intersection point of charged particle trajectories with this beam spot was checked and showed negligible residual systematics.

3. Event analysis

3.1. Hadronic event selection

Only charged particles measured in the tracking chambers and with a momentum p above 0.1 GeV/c, a measured track length over 50 cm and an angle to the beam axis exceeding 25° were used in this analysis.

The sum of the energies of these charged particles in each of the forward and backward hemispheres (with respect to the beams) was required to exceed 3 GeV, and the total energy had to be more than 15 GeV, assuming the pion mass for each particle. Furthermore, at least six charged particles were required with momenta over 0.2 GeV/c. These cuts selected 232 114 events as hadronic Z^0 decays.

After this hadronic event selection, the JADE jet clustering algorithm [5] was applied with a scaled invariant mass squared cut of 0.04. The mean number of jets per event was 2.39.

3.2. Charged particle selection

The charged particles from light hadron decays or from secondary interactions can confuse an attempt to find a secondary vertex close to the beam spot. To reduce this problem all pairs of oppositely charged particles were combined to see if they were consistent with a K_S^0 decay or γ conversion. About 0.1 K_S^0 and 0.25 γ per event were identified and the charged particles tagged so that they were not considered further.

After the jet finding and pair rejection, only charged particles with momentum over 0.5 GeV/c and lying within 40° of the jet axis were used in the subsequent analysis. Only jets with at least three such charged particles were accepted. All selected particles in the jet were required to have hits on at least two (of the three) different layers of the vertex detector, in order to be considered to be reliably measured. Only one jet in five met this requirement. Over half the loss of jets was due to purely geometric effects coming from the finite size of the vertex detector. The remaining loss was attributed to interactions in the material beyond the silicon, vertex detector inefficiencies and track fitting problems.

The effect of these two requirements on the data sample is listed in the first three rows of table 1. Also shown are the results of a full Monte Carlo simulation, starting from Z^0 decays generated by the program JETSET 7.3 [6] and including particle interactions in materials and detector resolutions [7]. The fractions of the four dominant B species assumed in this simulation can be seen in table 3 below; their lifetimes were all taken to be 1.2 ps except for the Λ_b^0 whose lifetimes was set at 1.3 ps.

Table 1
Cumulative effect of each selection on the 232 114 data and 369 609 simulated selected hadronic events.

Selection	Number of jets		
	data	simulation	ratio
initial jet sample	554484	878285	0.63
$\geqslant$ 3 charged particles per jet	499178	793053	0.63
each particle with $\geqslant$ 2 VD hits	96659	187199	0.52
not all from primary vertex	41941	72147	0.58
clear secondary vertex	6528	11502	0.57

It can be seen in table 1 that the requirement of 2 vertex detector hits on each charged particle was not well reproduced by the Monte Carlo simulation. This probably reflected the difficulty of reproducing particle reinteractions and track association. The probability of having two hits on any given particle track in the data was 96% to 99% of that in the simulation for momenta below 20 GeV/c; this fraction was lower for particles of higher momentum.

3.3. Calibration of track extrapolation errors

The assignment of particles to the primary vertex or B-hadron used the extrapolated track positions in the plane perpendicular to the beam direction. An accurate knowledge of the uncertainty on this extrapolation was therefore essential. The z coordinate was much less precise than $R\phi$, therefore the vertex reconstruction used only the $R\phi$ projection of the charged particle tracks with the z coordinate used to resolve ambiguities.

There were two contributions to the extrapolation error: the intrinsic measurement resolution (σ_{meas}) and the multiple scattering (σ_{scat}). The track extrapolation error, $\sigma_{R\phi}$, was parameterized by

$$\sigma_{R\phi} = \left(\sigma_{meas}^2 + \frac{\sigma_{scat}^2}{p^2 \sin^3 \theta}\right)^{1/2}, \qquad (1)$$

where p is the particle momentum in GeV/c and θ is its polar angle. The coefficients σ_{meas} and σ_{scat} were determined using the same charged particles as were used in the analysis. In all jets with at least four charged particles, the three particles of highest momentum and the three particles of lowest momentum were each taken to form a vertex, and the χ^2 probability, $P(\chi^2)$, that all three come from a common

point was found. This χ^2 probability was required to be greater than 0.2. The coefficients (σ_{meas}) and (σ_{scat}) were varied until a flat distribution was obtained for both the high and low momentum triplets. The high momentum distribution was more sensitive to the asymptotic uncertainty, and the low momentum distribution to the multiple scattering. The values obtained, $\sigma_{meas} = 30 \pm 3$ μm and $\sigma_{scat} = 70 \pm 4$ μm, represent an average over different classes of track, and are slightly larger than those in ref. [3], for which hits in all three silicon layers were required on each charged particle.

3.4. Secondary vertex identification

Particles had to be assigned to the correct vertex in order to determine the charge of the B-hadron. Each jet was examined independently. If produced by a b-quark it will in general contain several vertices: the primary interaction, b decay, c decay and perhaps s decay. However, in order to simplify the analysis, the jet was assumed to contain only the primary vertex and a single decay vertex. The flight distance of secondary charmed hadrons from B decay was thus ignored.

A vertex was formed from all selected particles in the jet constrained to pass through the measured beam spot, which was assumed to have a size of 150 μm by 10 μm. If there was a resolvable secondary vertex, then the χ^2 probability that all charged particle tracks come from a single vertex consistent with the beam spot was very small. Therefore, if the jet vertex had a χ^2 probability greater than 1% it was not considered further.

Next all the particles within the same jet were divided into two groups, with all possible permutations

being tried. One group was used to make a vertex which was constrained by the beam spot, while a secondary vertex was formed using the particles in the other group with no such constraint. At least two particles were required in the secondary vertex. The combined χ^2 probability, for which the number of degrees of freedom is the number of particles minus two, was required to exceed 1%. If there was one and only one combination which satisfied this requirement, a satisfactory secondary vertex was considered to have been found. Jets with more possible combinations were regarded as ambiguous, and rejected.

3.5. Secondary vertex selection

After these requirements (see table 1), the invariant mass at the secondary vertex, M_{vis}^π, was calculated, assuming that all charged particles were pions. Fig. 1 shows the mass distribution for data and Monte Carlo simulation, after all other selections have been applied, and with the simulated events subdivided into different quark flavours. A K_S^0 peak can be seen, because the criteria for their prior removal were very tight. The observed mass was less than the true mass
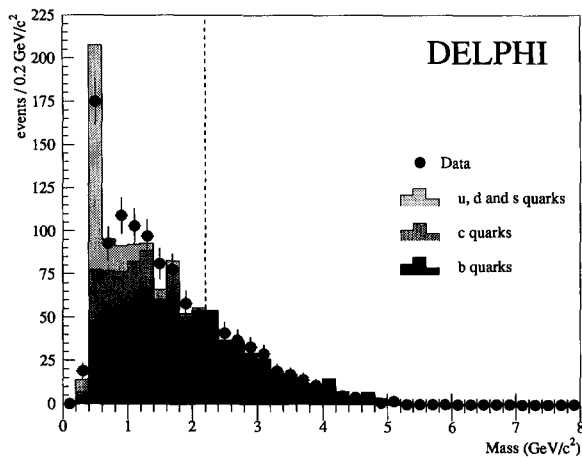

Fig. 1. The reconstructed mass, M_{vis}^π, for data and Monte Carlo simulation, with the cut at 2.2 GeV/c^2 indicated by the dashed line. The simulation has been weighted to correspond to a B lifetime of 1.5 ps and normalized to the same number of selected vertices as the data. All selections have been made except for the missing charged particle search and the mass cut. A residual peak of K_S^0 can be seen, because the rejection criteria were conservative.

because of the unused neutral particles and missing charged particles. On the basis of the observed distribution of the different quark flavours in the simulated sample, B decays were selected by requiring that M_{vis}^π be greater than 2.2 GeV/c^2. The absence of events above the kinematic limit at about the B^0 mass is consistent with the expectation of a correct assignment of particles to the vertices.

Table 2 shows this and the other selections explained below. It has two columns for the simulation in which generated B particles lifetimes were 1.2 ps except for the Λ_b^0 which was 1.3 ps. The first column, labelled unweighted, counts vertices in a straightforward manner, while in the second they are weighted to simulate a B-hadron lifetime of 1.5 ps. This weight is $W = (\tau_g/\tau_r)\exp(t/\tau_g - t/\tau_r)$, where τ_g is the generated lifetime, τ_r is the required lifetime and t is the proper time of the B decay. This procedure demonstrates the consistency of the selections if the mean B lifetime is around 1.5 ps.

The transverse distance between the two vertices, $l_{R\phi}$, was calculated, and its uncertainty, σ_l, was derived from the vertex errors. The vertices were used only if this uncertainty was less than 600 μm, to remove configurations with nearly parallel charged particle tracks. This rejected few B candidates, as their typical uncertainty was 190 μm.

Next, the vector sum of the momenta of all the particles assigned to the secondary vertex was found, and its azimuthal angle, ϕ_{mom}, obtained. Taking the azimuthal angle, ϕ_{geom}, of the vector joining the primary and secondary vertices, the difference $\delta\phi = \phi_{\text{mom}} - \phi_{\text{geom}}$ was computed. This was expected to be near zero for B candidates because the momentum will point in the same direction as the line of flight. However, ϕ_{mom} did not coincide with the B momentum, mostly due to the momentum carried by neutral particles. Furthermore, the measurement of the primary and secondary vertices produced an error on $\delta\phi$ which decreases with increasing decay length. The error, $\sigma_{\delta\phi}$, was parameterized from the Monte Carlo simulation as $\sqrt{0.033^2 + (140\ \mu\text{m}/l_{R\phi})^2}$. Only vertices with $\delta\phi/\sigma_{\delta\phi}$ less than three were accepted.

A comparison of these quantities and their errors in real and simulated data indicates that they are well modelled by the Monte Carlo simulation, as might be inferred from table 2. The following additional criteria were applied:

Table 2
Cumulated effect of each selection applied to the vertices. See section 3.5 for a discussion of the weighting procedure.

Selection	Number of vertices				
	data	unweighted		weighted	
		simulation	ratio	simulation	ratio
initial vertex sample	6528	11502	0.57	11881	0.55
mass > 2.2 GeV/c^2	544	744	0.73	935	0.58
$\sigma_l < 600$ μm	514	706	0.73	898	0.57
$\delta\phi/\sigma_{\delta\phi} < 3$	455	612	0.74	804	0.57
number of jets $\leqslant 3$	451	601	0.75	791	0.57
$l_{R\phi} < 4$ cm	436	568	0.77	758	0.58
$l_{R\phi}^{min} > 5\sigma_l$	428	566	0.76	756	0.57
$P(\chi^2) > 0.10$	265	360	0.74	496	0.53
no missing charged particle	253	341	0.74	473	0.53

– The number of jets in the event was required to be three or less, which reduced the chance of assigning the charged particles from a B decay to more than one jet. Note that if this happened the particle would have been ignored, and the charge would almost certainly be wrong. This rejected 1% of the events.

– The decay length, $l_{R\phi}$, was required to be less than 4 cm, well inside the beam pipe. This rejected 3% of events.

– The minimum acceptable decay length (see section 4.2.1) was more than 5 σ_l.

– The χ^2 probability of the accepted vertex combination was required to be greater than 10%, while preserving the previous criterion that no other combination should have a probability over 1%. A flat probability distribution is not expected for the correct assignment in B events, because of the decay length of the charmed hadrons. By requiring this large difference in probability, the chance of associating the wrong particles to the secondary vertex has been minimized.

The decay length distribution for the vertices finally selected is shown in fig. 2. The mean charged multiplicity of the accepted secondary vertices was 3.75 ± 0.08 for the data and 3.60 ± 0.07 for the Monte Carlo simulation. This showed agreement between simulation and data, but is not the mean charged particle multiplicity in B decay, which was 5.1 in the simulation. The difference is due to bias in the selections, not to losing 1.5 tracks per jet.
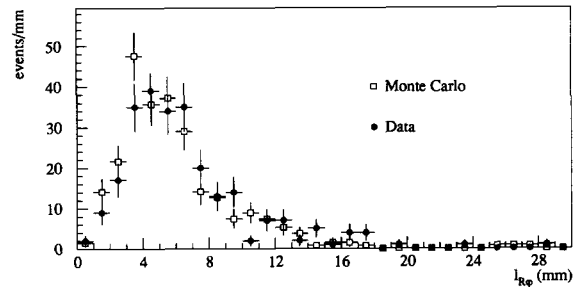
Fig. 2. The $R\phi$ decay lengths of the accepted events in Monte Carlo simulation and data.

3.6. Missing charged particle search

The analysis requires a good estimate of the charge of the decaying B-hadron, and so the loss of charged particles must be minimized. Hits in the vertex detector compatible with being produced by a particle coming from the B decay, but not associated to any particle track reconstructed by the main tracking chambers, are an indication of inefficiencies in the tracking system or interactions before the TPC. To avoid introducing an error in the measured charge, jets which contained such hits were removed as follows.

The vertex detector was searched for unassociated hits in all three layers which form a circle consistent with coming from the B decay point. The errors on the individual silicon points were considerably larger than the 8 μm previously stated since the z of the hypothetical particle was unknown, and the detector el-

ements were not perfectly parallel to the z axis. This led to an extrapolation precision, based on the vertex detector alone, of around 400 μm. A candidate particle formed in this way was therefore regarded as compatible with the B decay point if its distance of closest approach to that point was less than 1 mm. To be accepted it had to be within 40° in ϕ of the jet direction with a momentum to the beam direction, p_T, of more than 0.5 GeV/c.

The accuracy with which such a particle track was measured was not sufficient for it to be used in the analysis, and so if any were found the jet was discarded. This procedure rejected 5% of the jets, as can be seen in table 2.

3.7. Selected sample composition

The composition of the simulated events passing all the selections is listed in table 3. The fraction of B jets is estimated to be 98%. There is evidence of an enhancement in the selection of B^+ with respect to B^0 mesons. This could come from a variety of different effects, such as the longer D^+ lifetime as discussed later and the variation of efficiency with charged multiplicity, which peaks at a multiplicity of three and could favour charged B-hadrons. There must be a small enhancement in Λ_b^0 selection efficiency in the simulation arising from its longer lifetime, but this has been neglected throughout.

Table 3
The composition of the selected event sample in the Monte Carlo simulation, where all the B-hadron lifetimes are 1.2 ps except the Λ_b^0, which is 1.3 ps.

Type	Fraction of selected vertices (%)	Initial fraction of B-hadrons (%)
B^+	53 ± 4	40.1
B^0	30 ± 3	40.1
B_s^0	9 ± 2	11.9
Λ_b^0	6 ± 2	7.9
background	2 ± 1	–

4. Lifetime fitting procedure

4.1. Charge estimation

In order to extract the charged and neutral B lifetimes, it is important to estimate the charge at the detected secondary vertex as accurately as possible. A correction was made for undetected charged particles from B decays using the fraction of doubly and triply charged secondary vertices found. The procedure assumes the quark model prediction that there are no multiply-charged B-hadrons. The probability of getting the charge of the decaying particle wrong was fitted as

$$P(q \rightarrow Q) = \mathcal{P}^{|Q-q|} \frac{1 - \mathcal{P}}{1 + \mathcal{P}}, \qquad (2)$$

where q is the true charge, Q is the observed charge and $\mathcal{P}$ is a free parameter, which for small $\mathcal{P}$ is the probability of measuring a charge difference of one in either direction. This can be seen to be a reasonable description, as shown in fig. 3a. The charge was measured correctly in $71 \pm 3\%$ of the simulated events, and the numbers of multiply-charged vertices, shown in fig. 3b, were used to estimate the parameter $\mathcal{P}$ in the data (see table 4 below).

4.2. Proper time estimation

The B lifetime is fitted from the proper time distribution of the reconstructed decays. This requires a knowledge of the decay length and the B-hadron velocity. The former was found from the positions of the primary and secondary vertices; the latter was calculated from the measured momentum and invariant mass.
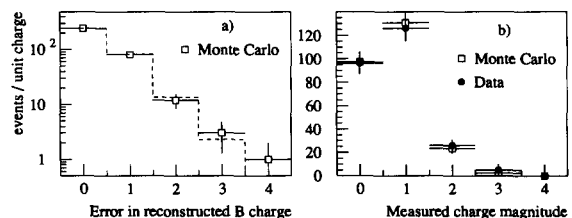

Fig. 3. (a) The modulus of the difference between the true charge and the reconstructed charge in Monte Carlo simulation, fitted using eq. (2). (b) The measured charge magnitude distribution including charged B-hadrons.

4.2.1. Decay length measurement

The measured decay length, $l_{R\phi}$, is a convolution of the decay length of the B-hadron with that due to the subsequent decays of B decay products, particularly D-mesons.

One of the selection criteria was that all particles assigned to the B should be compatible with coming from a single vertex and this requirement acted as a bias against the longer lived D-hadrons, particularly the D^+. The results of the simulation imply that the mean shift of the reconstructed vertex away from the real B decay point was 220 ± 30 μm and 320 ± 60 μm for D^0 and D^+ mesons, respectively. This should be contrasted with a factor 2.5 difference in the D lifetimes.

In fact, in order to extract the lifetime, the excess decay length, $l_{R\phi}^{\text{excess}}$, beyond the minimum required to identify the vertex, $l_{R\phi}^{\text{min}}$, was used rather than the full decay length, $l_{R\phi}$. The charged particle tracks identified as coming from the decay were moved back towards the primary interaction vertex without changing their relative positions. The point at which the decay vertex could just be distinguished with the procedure described above was found individually for each decay. The next best vertex combination has a probability of exactly 1% at this point. The distance to the primary vertex was then the minimum acceptable decay length, and the time distribution of the decaying particles beyond this point was just given by their lifetime.

While the change in the calculated proper time due to the finite decay time of the secondary D-hadrons is not completely removed for individual events, in this method it is significantly reduced. More important is that the influence of the D lifetime is not only to increase the apparent proper time of the events which would have been accepted in any case, but also to allow some events to be seen which would otherwise not have been accepted.

The minimum acceptable decay length of each event, as defined above, was required to be greater than 5 standard deviations σ_l. This selection ensures that an excess decay time distribution where resolution effects can be neglected and where the acceptance is constant is obtained. The excess decay time distribution can then be described by an exponential with a slope given by the B lifetime to a very good

approximation[#2].

The excess three dimensional decay length, l^{excess}, was found from this excess length in the $R\phi$ plane, $l_{R\phi}^{\text{excess}}$, as

$$l^{\text{excess}} = \frac{l_{R\phi}^{\text{excess}}}{\sin\theta}, \qquad (3)$$

where θ is the polar angle of the vector sum of the momenta of the charged particles assigned to the decay vertex.

4.2.2. Boost estimation

The momentum of the parent B was found using the method of ref. [8], which uses the fact that for sufficiently large boost, the velocity of the B is the same as that of the observed component:

$$\left(\frac{1}{P_B}\right)^{\text{est}} = \alpha \frac{M_{\text{vis}}^\pi}{M_B} \frac{1}{P_{\text{vis}}}, \qquad (4)$$

where $(1/P_B)^{\text{est}}$ is the estimate of the inverse of the B momentum, M_{vis}^π is the effective visible mass, assuming that all the particles are pions, P_{vis} is the sum of the momenta of the particles at the secondary vertex and α is a correction factor of order one. Substituting this into the equation for the excess proper time gives

$$t^{\text{excess}} = M_B l^{\text{excess}} \left(\frac{1}{P_B}\right)^{\text{est}} = \alpha \frac{M_{\text{vis}}^\pi l^{\text{excess}}}{P_{\text{vis}}}. \qquad (5)$$

The value of α used was $1.25 - 0.061 M_{\text{vis}}^\pi$ (GeV/c^2) for both charged and neutral B-hadrons. It deviated from one because of the exclusion of charged particles of momentum less than 0.5 GeV/c, the fact that M_{vis}^π was calculated on the assumption that all the particles were pions when it was very likely that at least one was a kaon, and the missing transverse momentum which biased the estimator for low momentum. The coefficients of α were derived from Monte Carlo simulation, and depended upon the B decay scheme assumed there. However, the dependence was rather weak.

The estimate of the proper time has statistical accuracy of 25% in the Monte Carlo simulation, and this

---

[#2] The convolution of an infinite exponential with an unknown (but finite) distribution is an exponential with the slope of the original.

increased the spread of the proper time distribution by a factor of $\sqrt{1 + 0.25^2} = 1.03$. The value of α had some dependence on the species, and was 3% smaller for B_s^0 and 1% larger for B-baryons in the simulation used. No correction was made for this effect.

The mean momentum of the accepted events, using eq. (4) and assuming that the mass of each B-hadron is 5.27 GeV/c^2, was found to be 33.4 ± 0.5 GeV/c for the data and 32.6 ± 0.5 GeV/c for the Monte Carlo simulation. Thus there is no apparent inconsistency when using an expression for α derived from simulated events.

4.3. The fit method

An unbinned maximum likelihood fit was made to the distribution of excess proper times. This included an estimation of the probability of reconstructing the charge wrongly, using the number of doubly and triply charged secondary vertices observed. The likelihood of event i to have observed charge Q_i and excess proper time t_i^{excess} was taken to be

$$\mathcal{L}_i = \sum_\nu P(q_\nu \to Q_i) C_\nu \exp(-t_i^{excess}/\tau_\nu), \qquad (6)$$

where the sum runs over the B-hadron species considered in the fit and over the background. The three fits considered later allow the species to be the average B, the charged and neutral B-hadrons, and the four most common species (B^+, B^0, B_s^0, Λ_b^0) at LEP, respectively. $P(q_\nu \to Q_i)$ is the probability that a B-hadron of charge q_ν will be reconstructed as having charge Q_i, C_ν is the normalization constant for species ν, and τ_ν is the mean lifetime of the B-hadrons from species ν.

$P(q_\nu \to Q_i)$ was given in eq. (2). It depended on the parameter $\mathcal{P}$, which was allowed to vary in the fit and was constrained by the observed number of multiply-charged events. The background fraction, seen to be 2% in table 3, was taken to have the charge distribution expected by combining four or five charged particles of random charge.

The normalization constants C_ν are given as

$$C_\nu = \frac{F_\nu}{\tau_\nu [1 - \exp(-t^{max}/\tau_\nu)]}, \qquad (7)$$

where the F_ν are the relative fractions of the various B species (and the background) in the selected sample,

and t^{max} is the maximum allowed excess proper time of the events used in the fit and was set to 8 ps. The fractions of the selected sample, F_ν, are related to the fractions f_ν which would have been observed if the lifetimes had been equal

$$F_\nu = \frac{1}{N} \sum_i \frac{f_\nu \exp(-t_i^{min}/\tau_\nu)}{\sum_\mu f_\mu \exp(-t_i^{min}/\tau_\mu)}, \qquad (8)$$

where N is the number of selected events and t_i^{min} is the proper time of the minimum decay distance at which event i would have been observed. The fractions f_ν are not the same as the production rates of the various B species because of of the different selection efficiencies for the different decay topologies, but are as given in table 3.

5. B lifetime results

5.1. Fit to mean B lifetime

In a first fit the charge information was ignored and all the data were fitted to give an average B lifetime. This average is not the usual mixture of species seen at LEP, but includes relatively more of the longer lived varieties. A background fraction of 2% with an apparent lifetime of 3.0 ps, which is simply a parameterization of the background seen in Monte Carlo simulation, was allowed in this fit. The result is

$$\langle \tau_B \rangle = 1.49 \pm 0.11 \,(\text{stat.}) \,\text{ps}. \qquad (9)$$

Applying the same treatment to simulated events gave $\langle \tau_B \rangle = 1.17 \pm 0.09$, while the mean B lifetime in the simulation was 1.21 ps. Fitting the reweighted events also gave good agreement, but the fluctuations in such fits were found to be bigger than the reported statistical errors, and so the results are not used.

Variation of the exact values of the cuts used did not give changes in the results larger than would have been expected statistically, and thus show no evidence for systematic effects. The major systematic error was therefore estimated as the same fractional size of effect as could be present without being seen in the simulated sample, 0.11 ps. A 3% systematic uncertainty in the momentum estimation was also allowed for,

coming from the difference between the value of α applicable for different B species. This gave a contribution to the systematic error of 0.05 ps. Finally, varying the background in the fit from zero to 4% changed the result by 0.02 ps. These have been combined to give

$$\langle \tau_B \rangle = 1.49 \pm 0.11 \,(\text{stat.}) \pm 0.12 \,(\text{syst.}) \text{ ps} . \qquad (10)$$

5.2. Fit to charged and neutral B-hadron lifetimes

The excess proper time distributions of the charged and neutral events are shown in fig. 4. The fit to the average charged and neutral B lifetimes, as described below, is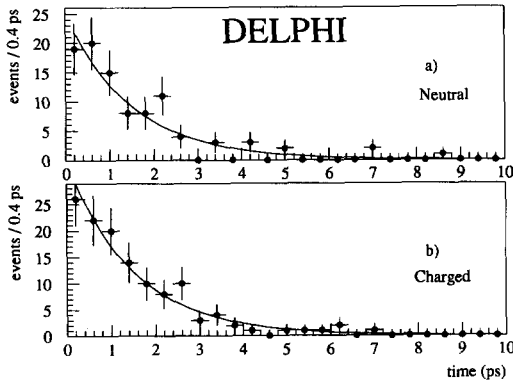 superimposed. In this fit it was assumed that all charged B species have one lifetime and all neutral ones have another. The relative normalization of the two species was left free to reduce the dependence upon the Monte Carlo simulation. The results of this fit are shown in table 4.

Table 5 shows the systematic uncertainties estimated in the analysis. The background fraction was varied from zero to double, and the changes interpreted as a systematic error. In the simulation the weighting technique was used to introduce different charged and neutral lifetimes. Then the ability of the fit program to recover those lifetimes was tested and a charge unfolding systematic error derived. This error is compatible with the Monte Carlo statistics, but such an effect cannot be excluded.

The momentum estimation includes not only the 0.05 ps coming from variation of α referred to in section 5.1, but also an allowance for a small bias in the value of α of events where a low momentum particle has been missed. Furthermore, variation of the parameter α in eq. (5) for different neutral B-hadrons leads to a systematic uncertainty on their lifetimes. The maximum variation of the α parameter between B species is 3%, and so this is the systematic uncertainty which is used.

The systematic assigned for any bias in the analysis was discussed in section 5.1 above; the systematic error on the ratio comes from the hypothesis that such a bias occurs for only one of the B species.

Variation of the exact values of the cuts used produced changes in the results compatible with the statistical fluctuations expected. These have therefore

Fig. 4. The excess proper time distributions of the charged and neutral events.

Table 4
Fit to average charged and neutral lifetimes, with the statistical errors shown. $\mathcal{P}$ is defined in section 4.1, and f_+ is the fraction of charged B-hadrons which would have been selected if the lifetimes had been equal. The lifetime ratio is not an independent parameter, but the errors have been calculated separately. The parameter $\mathcal{P}$ in the data corresponds to a 30% chance of getting the charge wrong. The B lifetime was 1.2 ps in the simulation, for all states except the Λ_b^0 for which it was 1.3 ps.

Parameter	Data	Simulation	
		fit result	correct value
$\langle \tau_{\text{charged}} \rangle$ (ps)	1.56 ± 0.19	1.13 ± 0.11	1.20
$\langle \tau_{\text{neutral}} \rangle$ (ps)	1.44 ± 0.21	1.34 ± 0.16	1.21
f_+	0.52 ± 0.08	0.63 ± 0.06	0.53
$\mathcal{P}$	0.18 ± 0.03	0.14 ± 0.02	0.16
$\langle \tau_{\text{charged}} \rangle / \langle \tau_{\text{neutral}} \rangle$	$1.09^{+0.28}_{-0.23}$	$0.84^{+0.17}_{-0.14}$	0.99

Table 5
Systematic uncertainties in the fit to the average charged and neutral B lifetimes.

Systematic	$\langle \tau_{charged} \rangle$ (ps)	$\langle \tau_{neutral} \rangle$ (ps)	$\langle \tau_{charged} \rangle / \langle \tau_{neutral} \rangle$
background fraction	±0.01	±0.01	±0.01
charge unfolding	±0.03	±0.05	±0.06
momentum estimation	±0.06	±0.06	±0.05
possible analysis bias	±0.11	±0.11	±0.07
total systematic	±0.13	±0.14	±0.11

not been quoted as systematic errors. The results for the mean charged and neutral lifetimes are

$$\langle \tau_{charged} \rangle = 1.56 \pm 0.19 (stat.) \pm 0.13 (syst.) \; ps \,,$$

$$\langle \tau_{neutral} \rangle = 1.44 \pm 0.21 (stat.) \pm 0.14 (syst.) \; ps \,,$$

$$\frac{\langle \tau_{charged} \rangle}{\langle \tau_{neutral} \rangle} = 1.09^{+0.28}_{-0.23} (stat.) \pm 0.11 (syst.) \,. \tag{11}$$

5.3. Fit to B^0 and B^+ lifetimes

The data were also interpreted in terms of the lifetimes of the B^0 and B^+ mesons, by assuming a composition for the neutral B-hadrons and also by using the lifetimes for the B_s^0 and Λ_b^0 as measured in independent analyses of LEP data. The B^0 lifetime extracted in such a manner depended critically upon these assumptions, but the B^+ was relatively insensitive to them. The B_s^0 and Λ_b^0 lifetimes were set to the average of ALEPH and DELPHI results: 1.05 ± 0.33 ps [9] and 0.98 ± 0.23 ps [10], respectively. The neutral species were divided in the same proportions as in table 3, and the relative amount of B^+ was fitted. No other B-hadrons were allowed for. The results are shown in table 6.

The systematic uncertainties have been taken from table 5, but rescaled appropriately. The systematic error on the composition of the sample, due to varying the B_s^0 and Λ_b^0 lifetimes by one standard deviation and to changing their fractions by a factor of two, has been added. The final values for the B^+ and B^0 meson lifetimes are

$$\tau_{B^+} = 1.56 \pm 0.19 (stat.) \pm 0.13 (syst.)$$

$$\pm 0.00 (composition) \; ps \,, \tag{12}$$

Table 6
Results for the B^+ and B^0 lifetimes; only statistical errors are quoted. The B lifetimes were set to 1.2 ps in the simulation for all states except the Λ_b^0 which was assigned a lifetime of 1.3 ps.

Parameter	Data value	Simulation
τ_{B^+} (ps)	1.56 ± 0.19	1.13 ± 0.11
τ_{B^0} (ps)	1.55 ± 0.25	1.41 ± 0.22
f_{B^+}	0.51 ± 0.08	0.63 ± 0.06
$\mathcal{P}$	0.18 ± 0.03	0.14 ± 0.02
τ_{B^+}/τ_{B^0}	$1.01^{+0.29}_{-0.22}$	$0.80^{+0.22}_{-0.15}$

$$\tau_{B^0} = 1.55 \pm 0.25 (stat.) \pm 0.17 (syst.)$$

$$^{+0.07}_{-0.06} (composition) \; ps \,,$$

$$\frac{\tau_{B^+}}{\tau_{B^0}} = 1.01^{+0.29}_{-0.22} (stat.) \pm 0.11 (syst.)$$

$$^{+0.04}_{-0.05} (composition) \,. \tag{12 cont'd}$$

Note that, if the four B lifetimes from this fit are combined to form a weighted LEP average, using the production fractions as given by the simulation, the result is $\langle \tau_B \rangle = 1.44$ ps, 0.05 ps lower than that deduced in section 5.1 because that sample was enriched in longer lived species.

6. Summary

From 232 114 hadronic Z^0 decays collected at the LEP collider with the DELPHI detector, a sample of 253 B-hadron candidates with an estimated purity of 98% has been extracted and the mean B lifetime has been measured to be

$$\langle \tau_B \rangle = 1.49 \pm 0.11 (stat.) \pm 0.12 (syst.) \; ps \,.$$

This result has somewhat larger errors than the $\langle \tau_B \rangle$ previously presented by DELPHI of 1.41 ± 0.07 ps [11], but is an independent number with different systematics. The mean presented here is over a mixture of events which contains more than the LEP average of the longest lived species, and is increased by about 0.05 ps as compared with that derived with some assumptions about the B_s^0 and Λ_b^0.

The results for the mean charged and neutral lifetimes are

$$\langle \tau_{\text{charged}} \rangle = 1.56 \pm 0.19 \,(\text{stat.}) \pm 0.13 \,(\text{syst.}) \text{ ps} ,$$

$$\langle \tau_{\text{neutral}} \rangle = 1.44 \pm 0.21 \,(\text{stat.}) \pm 0.14 \,(\text{syst.}) \text{ ps} ,$$

$$\frac{\langle \tau_{\text{charged}} \rangle}{\langle \tau_{\text{neutral}} \rangle} = 1.09^{+0.28}_{-0.23} \,(\text{stat.}) \pm 0.11 \,(\text{syst.}) .$$

The assumptions stated in the previous section allow the B^+ and B^0 lifetimes to be measured. Combining the systematic uncertainties, these are as follows:

$$\tau_{B^+} = 1.56 \pm 0.19 \,(\text{stat.}) \pm 0.13 \,(\text{syst.}) \text{ ps} ,$$

$$\tau_{B^0} = 1.55 \pm 0.25 \,(\text{stat.}) \pm 0.18 \,(\text{syst.}) \text{ ps} ,$$

$$\frac{\tau_{B^+}}{\tau_{B^0}} = 1.01^{+0.29}_{-0.22} \,(\text{stat.}) \pm 0.12 \,(\text{syst.}) .$$

A composition systematic uncertainty is taken into account for the B^0. The B^+ is assumed to completely dominate the charged state, so there is little composition uncertainty associated with its lifetime.

Previous measurements at CLEO and ARGUS [12] of the semi-leptonic branching ratios of the B^0 and B^+ mesons can be used to infer lifetimes which are equal to within about 25% if the semi-leptonic decay widths are assumed to be identical. DELPHI has previously measured the B^0 and B^+ lifetimes in an analysis based on Dl^- and D^*l^- events [13]. This gave $\tau_{B^0} = 1.17^{+0.29}_{-0.23} \pm 0.15 \pm 0.05$ ps, $\tau_{B^+} = 1.30^{+0.33}_{-0.29} \pm 0.15 \pm 0.05$ ps, $\tau_{B^+}/\tau_{B^0} = 1.11^{+0.51}_{-0.39} \pm 0.15 \pm 0.10$, in good agreement with other LEP measurements [14].

Acknowledgement

References

[1] G. Altarelli, R. Kleiss and Z. Verzegnassi, eds., Z physics at LEP 1, report CERN 89-08 (Geneva, 1989), Vol. 1, pp. 311–320.

[2] DELPHI Collab., P. Aarnio et al., Nucl. Instrum. Methods A 303 (1991) 233.

[3] N. Bingefors et al., The DELPHI Microvertex Detector, preprint CERN-PPE/92-173 (1992), Nucl. Instrum. Methods, to be published.

[4] D. Johnson, D. Reid and W. Trischuk, A beamspot database for lifetime measurements, DELPHI 92-36 PHYS 168 (Geneva, 18 March 1992).

[5] JADE Collab., W. Bartel et al., Z. Phys. C 33 (1986) 23.

[6] T. Sjöstrand, Comput. Phys. Commun. 39 (1986) 347; T. Sjöstrand and M. Bengtsson, Comput. Phys. Commun. 43 (1987) 367.

[7] DELSIM Reference Manual, DELPHI 87-98 PROG 100 (Geneva, July 1989).

[8] B. Franek, Rutherford Appleton Laboratory preprint RAL-85-026 (1985).

[9] DELPHI Collab., P. Abreu et al., Phys. Lett. B 289 (1992) 199; ALEPH Collab., D. Buskulic et al., A measurement of the B_s^0 lifetime, Proc. 7th Meeting of the American Physical Society, Division of Particle and Fields (DPF92) (Fermi National Accelerator Laboratory, USA, November 1992).

[10] DELPHI Collab., P. Abreu et al., Measurement of Λ_b^0 production and lifetime in Z^0 hadronic decays, preprint DELPHI 92-81 PHYS 192, Proc. 7th Meeting of the American Physical Society, Division of Particle and Fields (DPF92) (Fermi National Accelerator Laboratory, USA, November 1992); ALEPH Collab., D. Buskulic et al., Phys. Lett. B 297 (1992) 449.

[11] DELPHI Collab., P. Abreu et al., Inclusive measurement of the average lifetime of B-hadrons produced at the Z peak, preprint DELPHI 92-108, submitted to the XXVI Intern. Conf. on High energy physics (Dallas, TX, USA, August 1992).

[12] S. Stone, Semileptonic B decays: experimental, preprint HEPSY-4-91 (October 1991), in: B decays, ed. S. Stone (World Scientific, Singapore), to be published.

[13] DELPHI Collab., P. Abreu et al., Z. Phys. C 57 (1993) 181.

[14] OPAL Collab., P.D. Acton et al., Phys. Lett. B 307 (1993) 247; ALEPH Collab., D. Buskulic et al., Phys. Lett. B 307 (1993) 194.